The Canadian Mineralogist
Vol. 40, pp. 481-497 (2002)

PLATINUM-GROUP MINERALS IN CHROMITITE XENOLITHS FROM THE ONVERWACHT AND TWEEFONTEIN ULTRAMAFIC PIPES, EASTERN BUSHVELD COMPLEX, SOUTH AFRICA

FEDERICA ZACCARINI[§]

Via B. Ramazzini 15, I-41100 Modena, Italy

GIORGIO GARUTI[§]

Dipartimento di Scienze della Terra, Via S. Eufemia 19, I-41100 Modena, Italy

R. GRANT CAWTHORN[§]

Department of Geology, University of the Witwatersrand, PO Wits 2050, South Africa

ABSTRACT

The ultramafic pipes of Onverwacht and Tweefontein, in the eastern part of the Bushveld Complex, in South Africa, contain small xenoliths of chromitite that are believed to originate from the LG6 and MG4 chromitite layers, intersected during the emplacement of the pipes. Platinum-group minerals in the chromitite xenoliths consist of polyphase grains made up of: a) laurite along with unknown Ir–Ni–Fe sulfides and base-metal sulfides, occurring almost exclusively in fresh chromite (type-1 assemblage), b) abundant alloys (isoferroplatinum, ruthenium) and Rh–Pd–Ru arsenides (cherepanovite, ruthenarsenite, rhodarsenide, and palladodymite or palladoarsenide, polymorphs of Pd_2As), with accessory laurite and Pd antimonides (stibiopalladanite or sudburyite), included in both fresh chromite and interstitial olivine (type-2 assemblage), and c) relatively large grains of sperrylite and hollingworthite with minor laurite associated with the altered portions of the chromitite host (type-3 assemblage). Only assemblages of type 1 resemble the PGM observed in undisturbed LG6 and MG4 chromitite layers, in which laurite and minor cooperite are the dominant phases. The paucity of sulfides and the enrichment in alloys and As-rich phases make type-2 and type-3 assemblages more similar to the PGM associations reported from mineralized dunite in the platiniferous pipes, and metasomatized layers of chromitite adjacent to the pipes. These sulfur-poor assemblages of PGM are considered to have formed by metasomatic reaction of the chromitite with the volatile-rich component of the pipes over a range of temperatures, during and after the emplacement of the pipes.

Keywords: platinum-group minerals, chromitite, ultramafic pipes, Bushveld Complex, Republic of South Africa.

SOMMAIRE

Les pipes ultramafiques de Onverwacht et Tweefontein, dans la partie orientale du complexe de Bushveld, en Afrique du Sud, contiennent de petits xénolithes de chromitite qui auraient été dérivés des niveaux de chromitite LG6 et MG4, et détachés lors de la mise en place des pipes. Les minéraux du groupe du platine (MGP) de ces xénolithes définissent des associations à phases multiples: a) laurite avec sulfures méconnus contenant Ir–Ni–Fe et sulfures de métaux de base, presqu'exclusivement dans la chromite saine (assemblage de type 1), b) alliages abondants (isoferroplatine, ruthénium) et arséniures à Rh–Pd–Ru (chérépanovite, ruthenarsénite, rhodarsénide, et palladodymite ou palladoarsénide, polymorphes de Pd_2As), avec laurite et antimoniures de Pd (stibiopalladanite ou sudburyite) inclus soit dans la chromite saine, soit dans l'olivine interstitielle (assemblage de type 2), et c) sperrylite et hollingworthite en grains relativement grossiers, avec laurite accessoire, liées aux parties altérées de la chromitite hôte (assemblage de type 3). Seuls les assemblages de type 1 ressemblent aux minéraux du groupe du platine typiques des échantillons de chromitite LG6 et MG4 *in situ*, dans lesquels laurite et cooperite (phase mineure) sont prédominants. Par l'absence relative des sulfures et l'abondance des alliages et des phases arséniées, les assemblages de type 2 et 3 ressemblent davantage aux associations de MGP décrites dans la dunite minéralisée de pipes platinifères et les niveaux métasomatisés de chromitite près du contact avec les pipes. Ces assemblages à faible teneur en soufre auraient été formés par

§ *E-mail addresses*: email: fedezac@tsc4.com, garutig@unimo.it, 065rgc@cosmos.wits.ac.za

réaction métasomatique de la chromitite avec une composante enrichie en phase volatile issue des pipes sur un intervalle de températures, durant et après la mise en place des pipes.

(Traduit par la Rédaction)

Mots-clés: minéraux du groupe du platine, chromitite, pipes ultramafiques, complexe de Bushveld, République de l'Afrique du Sud.

Introduction

The Merensky Reef in the Bushveld Complex, in South Africa, was discovered at about the same time (1924) as platinum-bearing ultramafic pipes at Mooihoek, Driekop and Onverwacht, in the Critical Zone of the eastern part of the Bushveld (Figs. 1A, B) (Cawthorn 1999). However, the fact that these three bodies are pipe-like was not originally appreciated (Wagner & Mellor 1925), as they were considered part of an irregular layer within the normal layered sequence. The recognition of their pipe-like nature only became apparent as exploration progressed in late 1925. Thereafter, a number of discordant ultramafic pipes were discovered in the area, cutting all the zones of the layered sequence. Viljoen & Scoon (1985) classified all the pipes into "iron-rich ultramafic pegmatites", "non-platiniferous dunite", and "platiniferous magnesian dunite". They noted that the iron-rich pegmatites tend to predominate within and above the upper Critical Zone, whereas the magnesium-rich varieties seem to be restricted to the Lower and the lower Critical zones and the central sector of the upper Critical Zone (Fig. 1C). All the platiniferous bodies are located to the north of the Steelpoort fault (Fig. 1B). Generally, they consist of a core of iron-rich dunite to wehrlite, with $Fo_{43–73}$, embedded in magnesian dunite ($Fo_{>80}$) with or without an outer shell of wehrlite or clinopyroxenite (Stumpfl & Rucklidge 1982, Viljoen & Scoon 1985). Thus the inner and the outer zones of these platiniferous bodies were considered comparable to the iron-rich and magnesium-rich categories, respectively, but it was only where both facies were present that economic grades of mineralization were developed. Examples of the non-platiniferous magnesian dunite category were reported from the surroundings of the Clapham and Maandagshoek farms (northern sector of the eastern Bushveld, not shown in Fig.1B) typically characterized by a core of Mg-rich olivine ($Fo_{84–85}$) and orthopyroxene with a peripheral zone of wehrlite (Viljoen & Scoon 1985). Iron-rich pegmatites are numerous in the areas south of the Steelpoort fault. One pipe at Tweefontein (Fig. 1B), however, contains a core of dunite and harzburgite, in which the olivine is $Fo_{72–79}$, and a rim of clinopyroxenite in which the mg# reaches 86 (Tegner *et al.* 1994). Hence, this pipe falls between the magnesian dunite and iron-rich ultramafic bodies in the scheme of Viljoen & Scoon (1985). Be they magnesian, iron-rich or platiniferous, the pipes invariably have sharp, but extremely irregular, contacts with the layered rocks of the Critical Zone. They cut perpendicularly, and totally replace, the typical layering of pyroxenite, norite and anorthosite, but where chromite layers were intersected, fragments of chromitite were preserved in the dunite, possibly representing xenoliths or remnants of chromitite layers resistant to total replacement.

What is possibly the highest grade of platinum-group elements (PGE) mineralization ever published for a natural sample is one of 1213 dwt (pennyweight) per tonne (approximately 1700 ppm) reported by Wagner (1929) for a sample of chromitite from Onverwacht. However, the origin of such a remarkable grade remains enigmatic. All the knowledge concerning platinum-group minerals (PGM) in platiniferous pipes was derived almost exclusively from the study of concentrates and polished sections of mineralized dunite (Tarkian & Stumpfl 1975, Cabri & Chen 1976, Cabri *et al.* 1977a, b, c, Rudashevsky *et al.* 1992, and references therein), but no information is given in the literature about the presence of PGM in the fragments of chromitite.

In order to shed light on the reasons for this PGE enrichment, we have studied the mineralogy and textural relationships of PGM in fragments of chromitite from two ultramafic pipes, Onverwacht and Tweefontein. The assemblages of the PGM are compared with those from typical layers of chromitite that are considered to be the source of the fragments. According to field relationships and the stratigraphic position (Fig. 1C), the chromitite fragments hosted in the two pipes are believed to have been derived from the LG6 and MG4 chromitite layers, respectively (Wagner 1929, Tegner *et al.* 1994). With respect to the other platiniferous pipes, the Upper Group 2 (UG2) chromitite layer may have been intersected by the Driekop pipe, and the Mooihoek pipe may have intersected the Middle Group chromitite layers (Fig. 1C). Wagner (1929) made no mention of the presence of chromitites in either case. A few fragments of chromitite have been recorded from Driekop (Viljoen & Scoon 1985), but were not available for this study.

Geology of the Pipes

The Onverwacht pipe

A section through the Onverwacht pipe is shown in Figure 2, taken from Wagner (1929). Since the pipe was mined out by 1930, with subsequent access impossible,

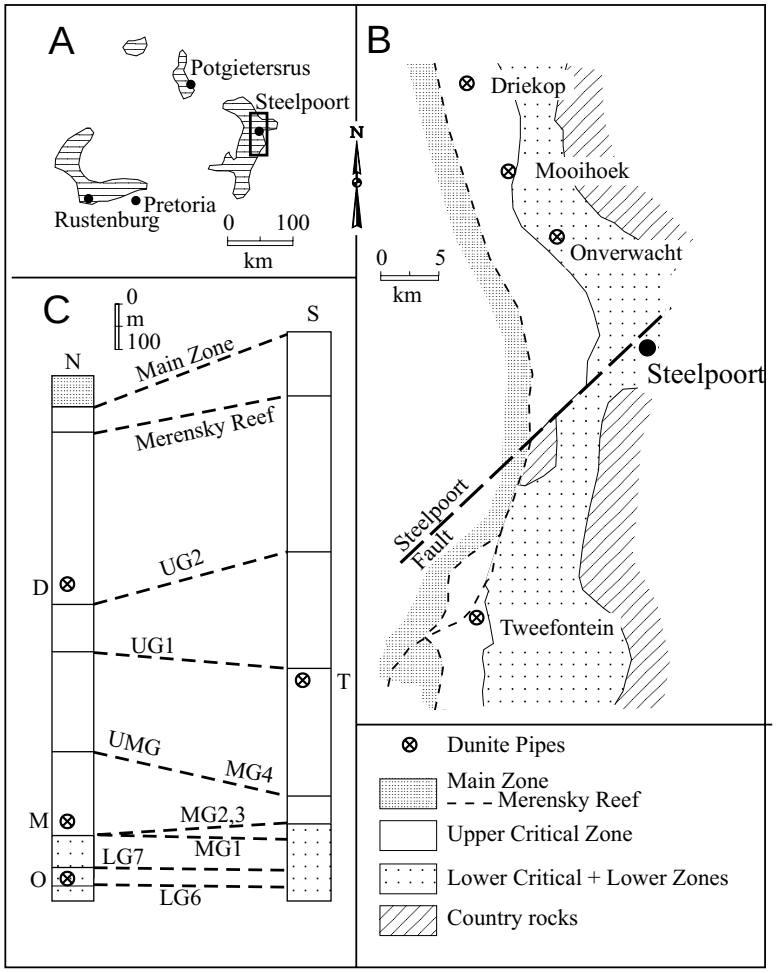

FIG. 1. A) location of the study area in the Bushveld Complex. B) Geological sketch-map of the eastern Bushveld Complex showing location of some relevant ultramafic pipes. C) Approximate stratigraphic position of the ultramafic pipes in relation with major layers of chromitite in the Lower (LG), Middle (MG), Upper Middle (UMG) and Upper groups (UG), within the Lower and Critical zones; O: Onverwacht, M: Mooihoek, T: Tweefontein, D: Driekop (modified after Viljoen & Scoon 1985).

no further information about the mineralized part of the pipe is available. The iron-rich dunite contained the bulk of the PGE mineralization, but parts of that rock type were barren, and ore-grade material did extend into the more magnesian dunite (Wagner 1929). Within the orebody, fragments of chromitite were found at various depths. Wagner specifically referred to samples at depths of 69.8 and 76.2 meters, but that is not necessarily the total range of occurrence. Considerable disruption of the original layer is implied. However, one aspect of this cross-section is now known to require additional explanation. In his original diagram, Wagner (1929) implied that the chromitite fragments were to be found at the approximate position where the extrapolation of the LG6 from surface outcrop was intersected by the pipe. As a result of mining the LG6 close to the pipe, it is now known that the LG6 plunges around the pipe, and that the outcrop of the LG6 close to the pipe is not at its normal regional position. Mining company information suggests that the geometrical relations are more likely to be as shown in Figure 2, and that the chromitite fragments occur close to the level of the collapsed LG6, although the exact location and dip of LG6 around the pipe are not known. A similar collapse-induced structure has been well documented for the Driekop pipe (Schiffries 1982), where the UG2 layer plunges steeply

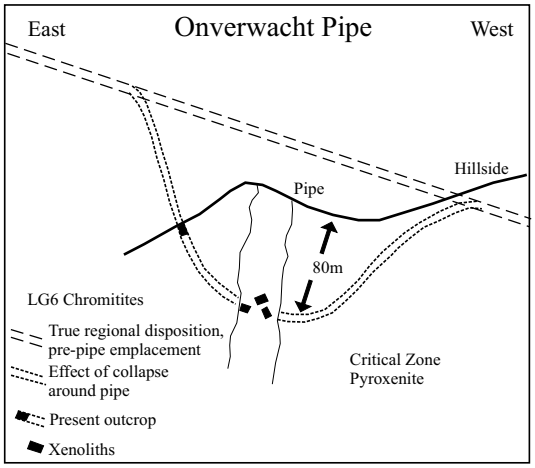

FIG. 2. East–west topographic section through the platiniferous ultramafic pipe of Onverwacht, showing the inferred relationships between the LG6 chromitite layer and the pipe body.

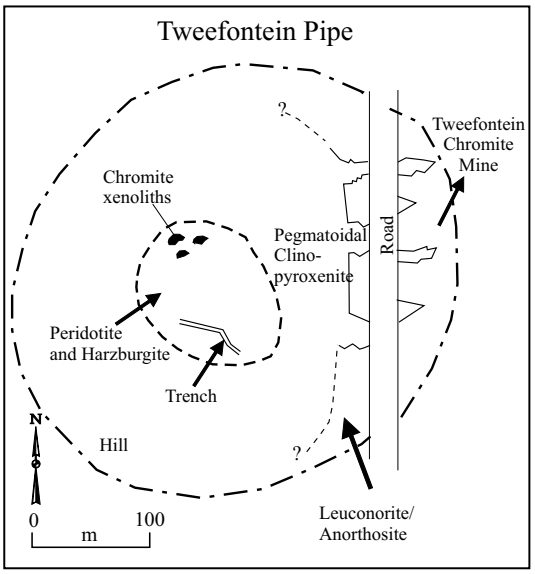

FIG. 3. Schematic plan of the Tweefontein pipe showing location of the chromitite xenoliths sampled inside the peridotite–harzburgite core, and the exposed external contact between the pegmatitic clinopyroxenite and the embedding leuconorite–anorthosite layers.

adjacent to the pipe. Its inferred intersection by the pipe lies below the level of mining. By analogy, it is probable that the Mooihoek pipe intersected the Middle Group chromitite layers, but details of the extent of any collapse around this pipe have not been documented.

The Tweefontein pipe

The geology of the Tweefontein pipe has been described by Tegner *et al.* (1994). Like most of these pipes, it occupies a topographic high about 300 m in diameter (Fig. 3), but the hillsides are covered with scree rather than good outcrop. A roadway cut through the edge of the pipe provides perfect exposure of the outer rim, which is dominated by irregular, near-vertical bodies of coarse clinopyroxenite cutting layered leuconorite and anorthosite. The contact between the outer pyroxenite and the inner peridotite and harzburgite is not exposed. The presence of orthopyroxene in harzburgite in the core makes it rather different from other pipes, where clinopyroxene is the more abundant pyroxene. A very old trench runs for 20 m across the top of the hill, and exposes harzburgite and peridotite, but the lack of any further development indicates that no PGE mineralization was found. Chromitite xenoliths are found in abundance on the north side of the hill, scattered over an area about 50 m^2. They are not angular, but have an irregular, amoeboid shape. The identity of the chromitite fragments in this pipe is uncertain. The implication of the geometry of Figure 3 is that the chromitite fragments ought to occur in the pipes close to the level at which the chromitite layer was intersected by the pipe. The nearest underlying and overlying chromitite layers are the MG4 and UG1 (see Fig. 1C); therefore, the chromitite fragments could represent MG material uplifted over about 125 m (Meadon 1995) or UG material displaced downward a few meters. Either way, fundamental displacement of the xenoliths relative to their original layer at Tweefontein is implied. On the basis of the relatively high Cr:Fe ratio in the chromite and the predominance of orthopyroxene over plagioclase in the silicate matrix of the Tweefontein chromitite, Tegner *et al.* (1994) argued that the xenoliths had been derived from the underlying MG4.

Distinctive field characteristics of platiniferous and barren pipes

There is one possibly significant unresolved geometrical difference between the platiniferous and barren pipes. The Onverwacht and Driekop pipes show evidence of collapse of the adjacent silicate layers around them (in the order of 100 m). The road cutting through Tweefontein clearly shows no distortion of the nearly flat-lying layering by the pipe (Tegner *et al.* 1994). Where these barren discordant pipes are intersected underground in mining operations, again minimal displacement is recorded (*e.g.*, Grimbeek 1995). It has been claimed that these bodies occur in the middle of potholes, and that there is some relationship to them. However, many pipes are not associated with potholes

and do not displace the layering (*e.g.*, Viljoen & Hieber 1986, Fig. 20), and below and above potholes the layering is not vertically displaced by the pipes (Viljoen & Hieber 1986, Fig. 13). It is possible that the mineralized pipes cause downward displacement, whereas unmineralized pipes do not.

Petrography of the Chromitite Xenoliths

The old mine dump at the Onverwacht pipe was carefully searched for chromitite fragments specifically for this project. The dump consists mainly of barren dunite from the outer portion of the pipe, since all ore from the inner portion was processed. Only two samples of chromitite (1200 and 1201) were found. They consist of amoeboid patches of chromite grains, intergrown with a gangue matrix that has different petrographic characters in the two samples. The gangue in sample 1200 consists of coarse-grained, undeformed olivine, affected by fracturing and weak serpentinization. Minute grains of chromite occur as drop-like inclusions in fresh olivine. In sample 1201, the gangue is mainly composed of serpentine, chlorite, and mixed Mg–Fe hydrous silicates and Fe hydroxides, in which rare relics of fresh olivine are preserved. Large patches of magnetite locally constitute the interstitial matrix to chromite grains, the texture suggesting that magnetite is replacing the chromian spinel. Sample 1201 is notable because it contains Cu-staining, suggestive of the original presence of sulfides, and is cut by thin veinlets of a colloform green–azure mineral identified by XRD as mcguinnessite: $(Mg,Cu)_2(CO)_3(OH)_2$. In both samples, 1200 and 1201, the chromite is heavily spotted with drop-like inclusions of clinopyroxene, amphibole and Na-rich phlogopite.

Two samples of chromitite (TW23 and BV27) from Tweefontein were newly collected for this study. They consist of a chromite cumulate in which oikocrysts of orthopyroxene with minor clinopyroxene, amphibole and plagioclase form the intercumulus material. Pyroxenes and amphibole locally occur as inclusions in the chromite. Secondary chlorite, "bastite" and Fe hydroxide occur along cracks and fractures as a result of late alteration.

Representative compositions of chromite from the investigated xenoliths are presented in Table 1, and compared with typical compositions of chromite from LG and MG chromitite layers. The chromite in the Onverwacht xenoliths is characterized by a remarkable decrease of Cr/Fe and Mg# and a higher TiO_2 content

TABLE 1. COMPOSITION OF CHROMITE IN THE ONVERWACHT AND TWEEFONTEIN CHROMITITE XENOLITHS AND THE UG1, MG1, MG4, LG6 CHROMITITE LAYERS

	Onverwacht			Tweefontein		LG6	MG4	MG1		UG1
Sample(s)	1200A	1200B	1201B	BV27C	TW23	$n = 16$	$n = 10$	BV26A	BV26C	$n = 8$
N	6	6	10	14	7	75	58	4	9	47
SiO_2 wt%	0.06	0.03	0.16	0.01	0.01			0.06	0.00	
TiO_2	0.95	1.34	2.72	1.03	0.98	0.58	0.77	0.65	0.62	1.07
Al_2O_3	15.56	14.06	15.33	19.27	20.07	13.92	17.50	16.25	15.08	15.26
FeO	26.11	27.00	31.28	23.92	23.99	18.93	20.13	19.97	21.39	22.35
Fe_2O_3	7.51	7.97	14.63	1.95	2.28	8.71	8.96	8.45	7.56	8.44
MgO	5.59	5.19	3.34	7.72	7.60	9.99	9.69	9.68	8.57	8.01
MnO	0.38	0.37	0.34	0.30	0.31	0.33	0.29	0.29	0.32	0.42
Cr_2O_3	43.00	43.68	31.35	45.88	44.01	47.37	42.42	44.55	46.23	44.26
NiO	0.13	0.09	0.11	0.02	0.09	0.11	0.13	0.11	0.00	0.15
ZnO	0.16	0.12	0.20		0.16					
V_2O_3	0.42	0.41	0.82		0.69					
Total	99.87	100.25	100.28	100.10	100.18	99.95	99.89	100.01	99.79	99.96
Cr/Fe	1.24	1.21	0.67	1.69	1.60	1.56	1.32	1.53	1.55	1.30
Mg#	0.28	0.25	0.16	0.36	0.36	0.49	0.46	0.46	0.42	0.39
Fe^{3+}#	0.10	0.11	0.21	0.02	0.03	0.11	0.11	0.10	0.09	0.11
Cr#	0.65	0.68	0.58	0.65	0.67	0.70	0.62	0.65	0.67	0.66

Samples BV26A and BV26C are from chromitite layer MG1 in the Tweefontein mine; LG6 (Scoon & Teigler 1994, 1995); UG1 and MG4 (Scoon & Teigler 1994). Sample(s): sample label or number (n) of analyzed samples. N: number of analyses made.

with respect to the original LG6 layer, differences that have been interpreted to result from re-equilibration by reaction with fluids producing the pipes (Stumpfl & Rucklidge 1982, Tegner *et al.* 1994). The xenoliths from Tweefontein do not exhibit such drastic change in the chromite composition and, as noted by Tegner *et al.* (1994), their Cr:Fe ratio is more compatible with a derivation from the underlying MG chromitite rather than the overlying UG chromitite layer.

Analytical Techniques

A total of 16 polished sections, four from each sample, were prepared and investigated for the presence of PGM. The PGM grains were located on polished section by reflected-light microscopy at 250–800× magnification, then they were investigated *in situ* by scanning electron microscopy (SEM) and characterized by electron-microprobe analysis at the University of Modena. Back-scattered electron (BSE) images were obtained using a Philips XL–40 instrument operated at 15–20 kV and 20 nA. The quantitative analyses were carried out using wavelength-dispersion spectrometry (WDS) with an ARL–SEMQ instrument, operated at 15 kV accelerating voltage and 10–20 nA beam current, with a beam diameter of 1 μm and counting times of 20 and 5 seconds for peak and backgrounds, respectively. On-line reduction of data was performed with the updated version 3.63, January 1996, of the PROBE software (Donovan & Rivers 1990), using natural magnesiochromite, the pure PGE metals, and synthetic SbS_2, NiAs, CoAsS, FeS_2, $CuFeS_2$ as standards. The following X-ray lines were used to analyze the PGM: *K*α for S, Cr, Fe, Cu, Co, and Ni, *L*α for Ir, Ru, Rh, Pt, Pd, Sb and As, and *M*α for Os. The calculation of detection limits for PGE and correction for the interferences Ru–Rh, Ir–Cu, and Rh–Pd are automatically performed for any single analysis by the PROBE software. Owing to the small size of the grains, usually close to the limits for quantitative determination, variable amounts of Cr and Fe were observed in a great number of analyzed grains, probably as result of secondary fluorescence or direct excitation of the host chromian spinel. Where necessary, the analytical results were therefore recalculated by subtracting all the Cr, and proportional amounts of Fe according to Cr:Fe ratio in the host spinel. Although this method may be not completely correct because of the differential absorption of Cr*K*α and Fe*K*α by the heavy PGE-rich matrix, it allowed us to estimate the possible presence of Fe in the PGM.

TABLE 2. MINERALOGY AND TEXTURE OF PGM INCLUSIONS IN CHROMITITE XENOLITHS FROM TWEEFONTEIN AND ONVERWACHT

Grain	Textural position	PGM assemblage	Fig.
		Onverwacht	
1200A 1	fresh chromite	ruthenarsenite	5A
1200A 2	fresh chromite	laurite	
1200A 3	chromite-silicate	laurite, Rh-Pt arsenide	
1200B 1	olivine	laurite, Pt_3Fe, Ru–Ir alloy, cherepanovite, $(Pd,Rh)_2(As,Sb)$	5B
1200B 2	olivine	laurite, Pt_3Fe, ruthenium, rhodarsenide	5C
1200B 3	chromite	Pt_3Fe, ruthenium	5F
1200C 1	ferrian chromite	sperrylite, laurite, magnetite	6A
1201A 1	altered matrix*	hollingworthite	6B
1201D 1	fresh chromite	laurite, Ru–Os–Ir alloy	4D
		Tweefontein	
TW23A 1	fresh chromite	laurite, Os-Ir alloy, ruthenian pentlandite, rutile	4E
TW23A 2	fresh chromite	laurite, ruthenium, Pt–Fe alloy, $(Pd,Rh)_2(As)$, ruthenarsenite, Pd–Sb, rutile	5D
TW23A 4	fresh chromite	laurite, Os–Ir–Ni sulfide	4F
TW23B 1	clinopyroxene	laurite	
TW23B 5	crack in chromite	laurite, Fe oxide, chlorite	
TW23B 6	crack in chromite	laurite, Pt–Fe alloy	
BV27B 1	crack in chromite	laurite	
BV27B 2	fresh chromite	Pt_3Fe	
BV27C 3a	fresh chromite	irarsite	
BV27C 3b	fresh chromite	laurite	
BV27C 4	fresh chromite	Pt_3Fe, Ru–Os–Ir–Pt alloy, $(Pd,Rh)_2(As)$	5E
BV27C 5	chromite–silicate	laurite, Pt–Fe alloy	4A
BV27C 6	fresh chromite	laurite, Os–Ir–Ni sulfide, amphibole	4B
BV27D 1	fresh chromite	laurite, chalcopyrite, pentlandite, bornite	4C
BV27D 4	chromite–silicate	Pt_3Fe, Pt–As, Rh–As–S	
BV27D 5	fresh chromite	ruthenium, Pd–Rh–As	

* altered matrix: chlorite, Fe oxides, mcguinnessite.

The Platinum-Group Minerals and Their Paragenetic Assemblages

All samples of chromitite from Onverwacht and Tweefontein were found to contain PGM, although only 25 grains were encountered in 10 of the 16 polished sections examined. In general, these grains are less than 10 μm across, although grains 20 and 200 μm across were observed in two cases. The PGM assemblage is characterized by the presence of all the six PGE occurring in a variety of mineral species: sulfides, alloys, arsenides, sulfarsenides, and one antimonide. These PGM generally form polyphase aggregates with or without base-metal sulfides and silicates; more rarely, they are found as single-phase crystals. Table 2 summarizes the textural position and mineralogy of the 25 PGM grains, whereas the results of the electron-microprobe analyses are presented in Tables 3 and 4. The lowest detection-limits obtained in all analytical runs are quoted in weight percent for single PGE in the footnotes to Table 3.

Close examination of Table 2 indicates that the PGM grains have at least three distinctive types of parageneses, illustrated in Figures 4 to 6. Type 1 occurs almost exclusively included in fresh chromite, and is dominated by sulfides. Laurite is the most common PGM, accompanied in turn by very subordinate Rh–Pt arsenide (not shown in figure) and Pt–Fe alloy (Fig. 4A), or associated with Ru–Os–Ir alloy (Fig. 4D), Ir–Ni–Fe sulfide (Figs. 4B, 4F), chalcopyrite – pentlandite – bornite (Fig. 4C), and ruthenian pentlandite plus osmium (Fig. 4E). The internal textures of the grains indicate that laurite may have crystallized in equilibrium with Ru–

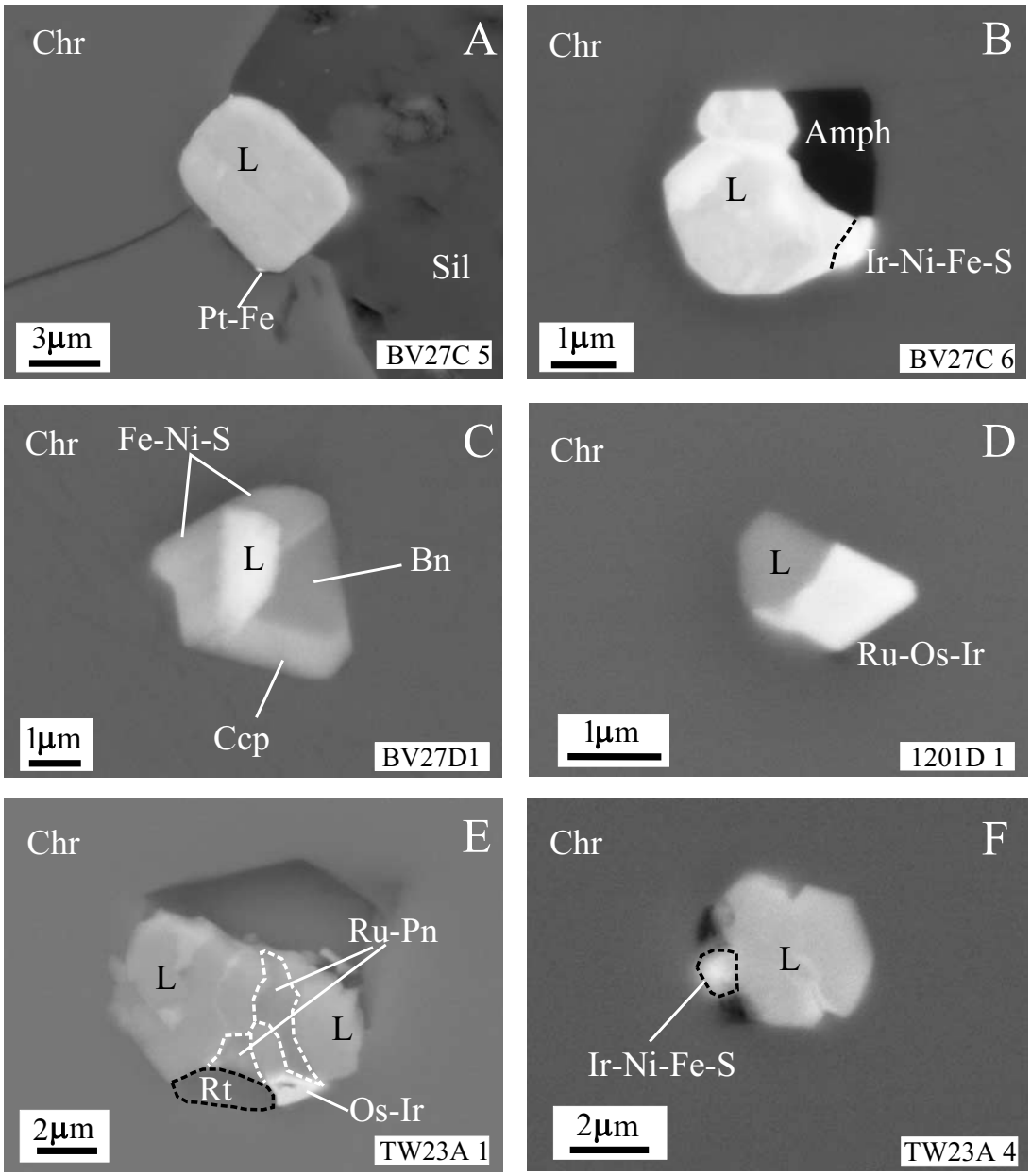

FIG. 4. Back-scattered electron (BSE) images of PGM inclusions of type-1 assemblages. A) Laurite associated with submicroscopic Pt–Fe alloy grain at the chromite–silicate contact (Tweefontein). B) Composite inclusion of laurite, Ir–Ni–Fe sulfide and amphibole. Note visible Os zonation in the laurite grain (Tweefontein). C) Laurite associated with bornite, chalcopyrite and Fe–Ni–S, possibly pentlandite (Tweefontein). D) Laurite and Ru–Os–Ir alloy (Onverwacht). E) Polyphase assemblage composed of zoned laurite, Os–Ir alloy, ruthenian pentlandite and rutile (Tweefontein). F) Zoned crystal of laurite with Ir–Ni–Fe sulfide (Tweefontein). Abbreviations: L: laurite, Bn: bornite, Ccp: chalcopyrite, Ru–Pn: ruthenian pentlandite, Rt: rutile, Chr: chromite, Sil: silicate, Amph: amphibole.

TABLE 3. REPRESENTATIVE COMPOSITIONS OF LAURITE IN CHROMITITES FROM ONVERWACHT AND TWEEFONTEIN

	Type	Os	Ir	Ru	Rh	Pt	Pd	Ni	Fe	Cu	S	As	Total
Onverwacht													
1200A 2 1	1	0.06	0.37	57.60	4.10	0.00	0.00	0.00	0.00	0.00	37.40	1.30	100.83
1200A 2 2	1	b.d.l.	0.23	58.40	3.10	0.00	0.00	0.00	0.00	0.00	36.80	1.00	99.53
1200A 3 1	1	0.32	2.68	53.02	2.14	0.49	2.99	n.a.	n.a.	n.a.	36.02	2.20	99.86
1200B 1 4*	2	0.24	0.71	53.20	2.80	0.32	0.62	0.05	0.00	0.04	31.30	1.70	90.98
1200B 1 5*	2	0.09	0.74	51.60	2.50	0.61	0.69	0.00	0.00	0.06	32.30	1.70	90.29
1200B 2 7*	2	0.78	0.64	57.60	2.10	0.00	0.00	0.04	0.00	0.05	32.34	1.10	94.65
1200C 1 4	3	6.10	b.d.l.	54.40	0.63	0.00	0.09	0.05	0.00	0.03	37.20	0.00	98.50
Tweefontein													
BV27C 5 1	1	6.62	4.77	44.81	1.97	2.41	0.56	0.02	0.03	0.07	34.82	3.18	99.26
BV27C 5 2	1	6.71	5.02	45.86	1.24	1.72	0.32	0.10	0.03	0.07	34.60	2.37	98.04
BV27C 5 3	1	6.58	3.08	49.05	0.85	1.64	0.25	0.00	0.00	0.07	35.23	1.93	98.68
BV27C 6 1	1	9.30	3.01	51.83	0.00	0.00	0.00	0.08	0.00	0.01	34.37	0.00	98.60
V27C 6 2	1	2.52	1.23	58.29	0.00	b.d.l.	0.00	0.04	0.00	0.05	37.37	0.00	99.50
TW23A 1 1	1	4.50	0.44	52.60	1.50	b.d.l.	1.10	0.49	0.17	0.31	37.70	0.00	98.81
TW23A 1 2	1	0.22	0.30	56.40	2.50	b.d.l.	0.00	0.63	0.32	0.00	39.10	0.00	99.47
TW23A 1 6	1	5.90	0.94	49.70	2.50	0.29	0.00	0.00	0.48	0.11	36.30	0.00	96.22
TW23A 4 1	1	2.70	0.77	57.00	0.79	0.00	0.00	0.42	0.07	0.77	37.40	0.00	99.92
TW23A 4 2*	1	4.30	1.00	49.30	0.56	0.00	0.00	0.30	0.00	0.24	31.70	0.00	87.40
TW23B 1 2	1	1.44	7.04	49.59	1.08	b.d.l.	2.08	n.a.	n.a.	n.a.	36.67	0.00	97.90
TW23B 5 6	1	18.23	1.25	38.83	2.61	0.28	1.56	n.a.	n.a.	n.a.	36.49	0.19	99.44
TW23B 5 7	1	3.07	4.64	49.98	2.68	b.d.l.	2.23	n.a.	n.a.	n.a.	38.14	0.00	100.74
TW23B 6 4	1	1.89	2.37	50.41	3.17	0.93	1.08	n.a.	n.a.	n.a.	36.23	1.91	97.99
Onverwacht													
1200A 2 1	1	0.02	0.11	31.74	2.22	0.00	0.00	0.00	0.00	0.00	64.95	0.97	
1200A 2 2	1	b.d.l.	0.07	32.64	1.70	0.00	0.00	0.00	0.00	0.00	64.84	0.75	
1200A 3 1	1	0.10	0.80	30.07	1.19	0.14	1.61	n.a.	n.a.	n.a.	64.40	1.68	
1200B 1 4*	2	0.08	0.24	33.60	1.74	0.10	0.37	0.05	0.00	0.04	62.32	1.45	
1200B 1 5*	2	0.03	0.24	32.32	1.54	0.20	0.41	0.00	0.00	0.06	63.77	1.44	
1200B 2 7*	2	0.25	0.21	35.12	1.26	0.00	0.00	0.04	0.00	0.05	62.16	0.90	
1200C 1 4	3	1.84	b.d.l.	30.96	0.35	0.00	0.05	0.05	0.00	0.03	66.72	0.00	
Tweefontein													
BV27C 5 1	1	2.08	1.49	26.55	1.15	0.74	0.32	0.02	0.03	0.07	65.02	2.54	
BV27C 5 2	1	2.13	1.58	27.45	0.73	0.53	0.18	0.10	0.03	0.07	65.28	1.91	
BV27C 5 3	1	2.06	0.95	28.88	0.49	0.50	0.14	0.00	0.00	0.07	65.38	1.53	
BV27C 6 1	1	2.96	0.95	31.06	0.00	0.00	0.00	0.08	0.00	0.01	64.93	0.00	
BV27C 6 2	1	0.75	0.36	32.71	0.00	b.d.l.	0.00	0.04	0.00	0.04	66.10	0.00	
TW23A 1 1	1	1.34	0.13	29.51	0.83	b.d.l.	0.59	0.47	0.17	0.28	66.68	0.00	
TW23A 1 2	1	0.06	0.09	30.65	1.33	b.d.l.	0.00	0.59	0.31	0.00	66.97	0.00	
TW23A 1 6	1	1.83	0.29	29.00	1.43	0.09	0.00	0.00	0.51	0.10	66.76	0.00	
TW23A 4 1	1	0.80	0.23	31.74	0.43	0.00	0.00	0.40	0.07	0.68	65.65	0.00	
TW23A 4 2*	1	1.49	0.34	32.12	0.36	0.00	0.00	0.34	0.00	0.25	65.10	0.00	
TW23B 1 2	1	0.44	2.14	28.72	0.61	b.d.l.	1.14	n.a.	n.a.	n.a.	66.94	0.00	
TW23B 5 6	1	5.74	0.39	23.03	1.52	0.09	0.88	n.a.	n.a.	n.a.	68.20	0.15	
TW23B 5 7	1	0.91	1.36	27.92	1.47	b.d.l.	1.18	n.a.	n.a.	n.a.	67.15	0.00	
TW23B 6 4	1	0.58	0.72	28.96	1.79	0.28	0.59	n.a.	n.a.	n.a.	65.61	1.48	

Results of electron-microprobe analyses, quoted in weight % above and in terms of atom proportions below. Type: 1: sulfide-rich assemblage, 2: sulfide-poor assemblage, 3: secondary (see text for explanation). *: results of semiquantitative analyses; n.a.: not analyzed; b.d.l.: below detection limit. Detection limits (in wt%): 0.06% Os, 0.23% Ir, 0.05% Ru, 0.28% Rh, 0.26% Pt, 0.05% Pd.

TABLE 4. REPRESENTATIVE COMPOSITIONS OF PGM IN CHROMITITES FROM ONVERWACHT AND TWEEFONTEIN

		Os	Ir	Ru	Rh	Pt	Pd	Ni	Fe	Cu	S	As	Sb	Total
Arsenides														
1200B 1 8	$(Pd,Rh)_2(As,Sb)$	0.10	0.00	0.00	33.90	0.00	35.40	0.33	0.00	0.28	0.00	18.10	10.90	99.01
BV27C 4 3	$(Pd,Rh)_2(As)$	0.44	b.d.l.	0.79	33.13	b.d.l.	40.49	0.06	0.01	0.03	0.00	25.11	n.a.	100.06
TW23A 2 1	$(Pd,Rh)_2(As)$	0.00	0.00	2.30	25.50	0.86	42.30	0.58	0.00	0.00	0.00	26.00	n.a.	97.54
1200B 2 6	rhodarsenide	0.36	0.43	0.62	55.50	b.d.l.	12.50	0.34	0.87	0.05	0.03	26.30	n.a.	97.00
1200A 1 2	ruthenarsenite	0.00	1.10	39.30	17.00	b.d.l.	0.00	0.71	0.00	0.00	0.09	41.90	n.a.	100.10
TW23A 2 2	ruthenarsenite	b.d.l.	0.00	31.90	23.30	0.77	1.10	0.24	0.00	0.00	0.62	40.00	n.a.	97.93
1200B 1 10	cherepanovite	0.16	0.44	25.50	29.90	0.60	0.00	0.08	0.00	0.06	0.00	41.50	n.a.	98.24
1200C 1 1	sperrylite core	0.15	0.39	0.47	1.20	55.50	0.00	0.00	0.00	0.00	0.15	43.30	n.a.	101.16
1200C 1 3	sperrylite rim	0.16	b.d.l.	0.59	0.38	54.40	b.d.l.	0.00	0.00	0.00	0.21	43.20	n.a.	98.94
Sulfarsenide														
1201A 1 2	hollingworthite	5.60	0.26	2.80	31.60	12.20	0.58	0.00	0.00	0.00	13.00	34.40	n.a.	100.44
1201A 1 4	hollingworthite	3.20	0.00	1.50	35.40	10.30	0.89	0.00	0.00	0.00	13.50	35.70	n.a.	100.49
Alloys														
1200B 2 3	ruthenium	7.40	13.40	64.50	2.75	10.70	0.00	0.08	0.00	0.00	0.00	0.00	n.a.	98.83
TW23A 2 3	ruthenium	12.90	6.20	70.00	1.60	9.60	0.00	0.08	0.16	0.03	0.00	0.00	n.a.	100.57
1200B 1 1	Pt_3Fe	0.16	0.84	0.18	1.10	85.10	0.05	0.78	10.80	0.52	0.00	0.00	n.a.	99.53
1200B 2 5	Pt_3Fe	0.00	0.65	0.29	2.30	83.70	0.34	0.78	11.50	0.48	0.00	0.00	n.a.	100.04
1200B 3	Pt_3Fe	0.55	0.51	0.22	6.39	78.04	0.92	0.92	11.30	0.44	n.a.	n.a.	n.a.	99.29
BV27B 2	Pt_3Fe	0.34	b.d.l.	0.00	0.94	84.29	1.40	0.49	10.74	0.43	n.a.	n.a.	n.a.	98.63
BV27C 4 4	Pt_3Fe	0.60	0.45	0.13	5.74	77.66	4.79	0.41	9.22	0.36	0.00	0.00	n.a.	99.36
BV27D 4	Pt_3Fe	0.00	b.d.l.	0.00	1.67	85.43	0.96	0.47	9.82	0.48	n.a.	n.a.	n.a.	98.83
Arsenides														
1200B 1 8	$(Pd,Rh)_2(As,Sb)$	0.05	0.00	0.00	32.82	0.00	33.14	0.56	0.00	0.44	0.00	24.07	8.92	
BV27C 4 3	$(Pd,Rh)_2(As)$	0.22	0.00	0.74	30.66	0.00	36.30	0.10	0.02	0.04	0.00	31.92	n.a.	
TW23A 2 1	$(Pd,Rh)_2(As)$	0.00	0.00	2.21	24.07	0.43	38.62	0.96	0.00	0.00	0.00	33.71	n.a.	
1200B 2 6	rhodarsenide	0.18	0.21	0.59	51.80	0.00	11.28	0.56	1.50	0.08	0.09	33.72	n.a.	
1200A 1 2	ruthenarsenite	0.00	0.50	34.27	14.56	0.00	0.00	1.07	0.00	0.00	0.25	49.35	n.a.	
TW23A 2 2	ruthenarsenite	0.00	0.00	28.34	20.33	0.35	0.93	0.37	0.00	0.00	1.74	47.95	n.a.	
1200B 1 10	cherepanovite	0.08	0.21	22.83	26.29	0.28	0.00	0.12	0.00	0.09	0.00	50.12	n.a.	
1200C 1 1	sperrylite core	0.09	0.23	0.52	1.32	32.10	0.00	0.00	0.00	0.00	0.53	65.21	n.a.	
1200C 1 3	sperrylite rim	0.10	0.00	0.67	0.42	32.04	0.00	0.00	0.00	0.00	0.75	66.02	n.a.	
Sulfarsenide														
1201A 1 2	hollingworthite	2.27	0.10	2.13	23.65	4.82	0.42	0.00	0.00	0.00	31.23	35.37	n.a.	
1201A 1 4	hollingworthite	1.26	0.00	1.11	25.78	3.96	0.63	0.00	0.00	0.00	31.55	35.71	n.a.	
Alloys														
1200B 2 3	ruthenium	4.69	8.40	76.91	3.22	6.61	0.00	0.16	0.00	0.00	0.00	0.00	n.a.	
TW23A 2 3	ruthenium	7.87	3.74	80.34	1.80	5.71	0.00	0.16	0.33	0.05	0.00	0.00	n.a.	
1200B 1 1	Pt_3Fe	0.13	0.65	0.27	1.60	65.19	0.06	1.99	28.90	1.22	0.00	0.00	n.a.	
1200B 2 5	Pt_3Fe	0.00	0.49	0.42	3.25	62.39	0.46	1.93	29.95	1.10	0.00	0.00	n.a.	
1200B 3	Pt_3Fe	0.41	0.38	0.31	8.83	56.87	1.23	2.23	28.77	0.98	n.a.	n.a.	n.a.	
BV27B 2	Pt_3Fe	0.27	0.00	0.00	1.38	65.11	1.98	1.26	28.98	1.02	n.a.	n.a.	n.a.	
BV27C 4 4	Pt_3Fe	0.46	0.34	0.19	8.16	58.25	6.59	1.02	24.16	0.83	0.00	0.00	n.a.	
BV27D 4	Pt_3Fe	0.00	0.00	0.00	2.48	66.90	1.38	1.22	26.86	1.15	n.a.	n.a.	n.a.	

Results of electron-microprobe analyses, quoted in weight % above and in terms of atom proportions below. n.a.: not analyzed, b.d.l.: below detection limit. Detection limits as stated in Table 3. Samples TW23 and BV27 are from Tweefontein, and samples 1200 and 1201 are from Onverwacht.

Os–Ir; according to the experimental results of Brenan & Andrews (2001), this paragenesis is typical of a very high temperature and the absence of an immiscible sulfide liquid. In contrast, the Ir–Ni–Fe and base-metal sulfides formed later, overgrew pre-existing laurite, and may have reacted in some case with the ruthenium disulfide. Amphibole and rutile have been identified as occasional constituents of the polyphase inclusions (Figs. 4B, E).

Type 2 is indifferently found in chromite or olivine, and is characterized by a paucity of sulfides (only minor laurite) and a significant predominance of PGE alloy (ruthenium, Pt_3Fe, and unidentified Pt–Fe alloys), Rh–Ru–Pd arsenides (cherepanovite, rhodarsenide, palladoarsenide or palladodymite, and ruthenarsenite), with accessory irarsite and one unidentified Pd antimonide. The Pt–Fe alloy and ruthenium form lamellar intergrowths that may indicate unmixing from an original homogeneous Pt–Ru–Fe alloy (Figs. 5B, E, F). The marginal location of the arsenides and laurite with respect to the alloys in the composite inclusion (Figs.5B, C, D, E) suggest an order of crystallization alloy – arsenide – sulfide, although the very constant association in this type of inclusions may also indicate that the entire assemblage was derived by the subsolidus equilibration of a high-temperature PGE–As–S–Sb compound. On the other hand, the fact that Pt_3Fe alloy (*i.e.*, grain BV27B 2, Table 2), ruthenarsenite (Fig. 5A) and irarsite also were encountered as single-phase inclusions in the chromite indicates that these PGM may have crystallized as independent phases at a high temperature.

Type 3 consists of As-bearing PGM characterized by both a relatively large grain-size (20–200 μm) and close association with secondary silicates and oxides. In one example, a grain of sperrylite is associated with accessory laurite and magnetite in the altered portion of a chromite crystal in contact with ferrian chromite and serpentine (Fig. 6A). In another case, one polygonal grain of hollingworthite (Fig. 6B) seems cracked and veined by Fe oxides or hydroxides, whereas the including matrix consists of an irresolvable mixture of Mg–Fe hydrous silicates, Fe hydroxides and mcguinnessite (Table 2).

Composition of the Platinum-Group Minerals

Laurite

The laurite contains minor amounts of Os (up to 5.74 at.%), Ir (up to 2.14 at.%), Rh (up to 2.22 at.%) and Pd (up to 1.61 at.%), whereas Pt occurs in traces only; two grains of laurite associated with small particles of Pt–Fe alloy (Fig. 4A, anal. BV27C–5–1, BV27C–5–2, BV27C–5–3, and TW23B–6–4, Table 3) exceptionally contain 0.74 and 0.28 at.% Pt, respectively. Measurable amounts of As (from 0.15 to 2.54 at.%) were detected in some grains, apparently unrelated to either textural position or paragenetic association of the laurite. Most grains proved to be compositionally homogeneous, although in three examples of the type-1 assemblage, laurite shows patchy zoning (Figs. 4B, E, F) corresponding to variations in Os content (anal. BV27C–6–1, BV27C–6–2, TW23A–1–1, TW23A–1–2, TW23A–1–6, TW23A–4–1, TW23A–4–2, TW23B–5–6, TW23B–5–7, Table 3).

Unknown Ir–Ni–Fe sulfide

The grains of unknown Ir–Ni–Fe sulfides in Figures 4B and 4F were found to be too small for reliable quantitative analysis; X-ray spectra indicate Ir as the main constituent, along with Ni and Fe in decreasing order of abundance, and Os in trace amounts.

Ruthenian pentlandite

Ruthenian pentlandite (Fig. 4E) was qualitatively identified. On the basis of repeated X-ray spectra obtained from this mineral, we exclude the possibility that Ru results from fluorescence from the adjacent laurite.

Pt–Fe alloy

Only the Pt–Fe alloy from polyphase inclusions of type 2 (Figs. 5B, C, E, F) could be quantitatively analyzed. The grains show a variable stoichiometry, between $Pt_{2.68}Fe_{1.16}Ni_{0.08}Cu_{0.05}$ and $Pt_{2.96}Fe_{0.97}Ni_{0.04}Cu_{0.03}$ (anal. 1200B–1–1, 1200B–2–5, 1200B–3–1 and BV27C–4–4, Table 4). Variable amounts of Rh (1.38–8.83 at.%), Pd (0.46–6.59 at.%), Ni (1.02–2.23 at.%) and Cu (0.83–1.22 at.%) were observed substituting for Pt and Fe. In spite of a slight deficiency in Pt, compositions of these alloys are consistent with isoferroplatinum (ideal formula Pt_3Fe), although unequivocal attribution to this species requires determination of the crystal structure (Cabri & Feather 1975).

Ruthenium alloy

Grains of ruthenium alloy from type-2 polyphase inclusions shown in Figures 5C and 5D were analyzed. Both compositions (anal. 1200B–2–3 and TW23A–2–3, Table 4) can be ascribed to the species ruthenium (Harris & Cabri 1991), although the grain hosted in chromite ($Ru_{0.8}Os_{0.08}Pt_{0.06}Ir_{0.04}Rh_{0.02}$) displays lower Ir content than that included in olivine ($Ru_{0.77}Ir_{0.08}Pt_{0.07}Os_{0.05}Rh_{0.03}$). Ruthenium lamellae within the isoferroplatinum on Figure 5F were identified only qualitatively.

Unidentified Ru–Os–Ir alloy

The Ru–Os–Ir and Os–Ir alloys in type-1 composite inclusions (Figs. 4D, E) are too small for reliable electron-microprobe analysis. On the basis of dominant PGE, they were attributed to the species ruthenium and osmium, respectively.

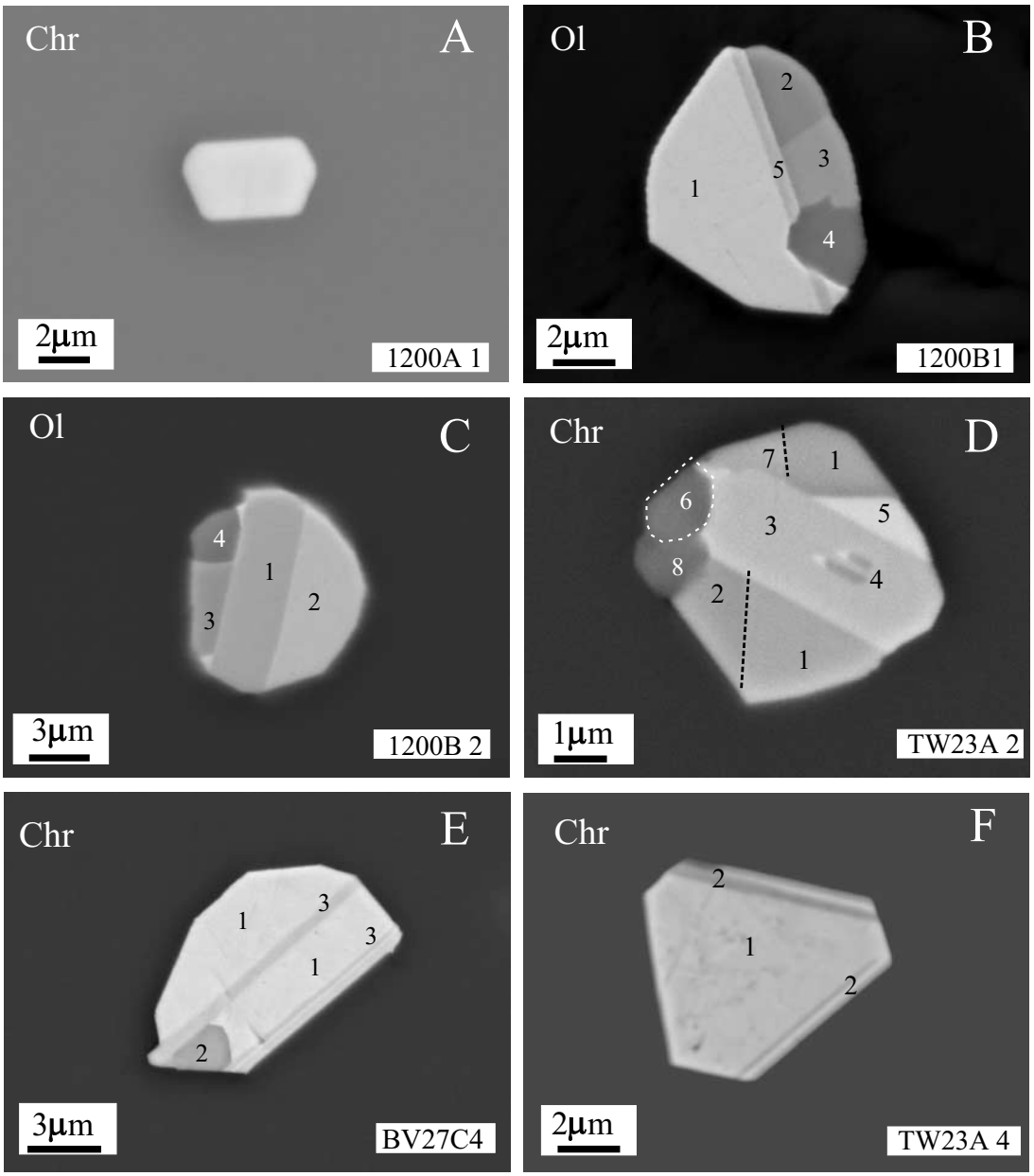

FIG. 5. BSE images of PGM inclusions of type-2 assemblages. A) Single-phase Rh-rich ruthenarsenite (Onverwacht). B) Composite PGM inclusion: 1: Pt_3Fe, 2: Ru-rich cherepanovite, 3: $(Pd,Rh)_2(As,Sb)$, 4: laurite, 5: Ru–Os–Ir alloy (Onverwacht). C) Composite PGM inclusion: 1: ruthenium, 2: Pt_3Fe, 3: Pd-rich rhodarsenide, 4: laurite (Onverwacht). D) Composite PGM inclusion: 1: $(Pd,Rh)_2As$, 2: Rh-rich ruthenarsenite, 3: ruthenium, 4: small inclusions of Pd–Rh–As, 5: Pt–Fe alloy, 6: laurite, 7: Pd–Sb, 8: rutile (Tweefontein). E) Composite PGM inclusion: 1: Pt_3Fe, 2: $(Pd,Rh)_2As$, 3: Ru–Os–Ir alloy (Tweefontein). F) Composite PGM inclusion: 1: Pt_3Fe, 2: ruthenium lamellae (Onverwacht). Abbreviations: Ol: olivine, Chr: chromite.

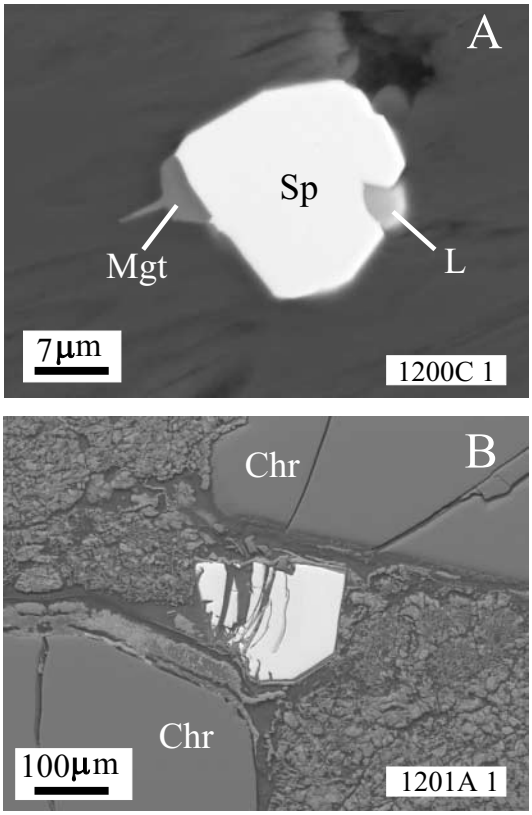

FIG. 6. BSE images of PGM of type-3 assemblages. A) Sperrylite associated with laurite and magnetite in altered chromite (dark gray) and serpentine (black) (Onverwacht). B) Cracked hollingworthite veined with Fe oxides in a matrix of chlorite, Fe oxides and mcguinnessite (Onverwacht). Abbreviations: Sp: sperrylite, L: laurite, Mgt: magnetite, Chr: chromite.

Ru–Rh–Pd arsenides

The Ru–Rh–Pd arsenides encountered in inclusions of type 2 have stoichiometries clustering around X_2As and XAs. The metal-excess compounds have compositions intermediate between rhodarsenide (orthorhombic Rh_2As as defined by Tarkian *et al.* 1997) and palladoarsenide (monoclinic Pd_2As: Begizov *et al.* 1974, Cabri *et al.* 1975) or palladodymite (orthorhombic dimorph of Pd_2As Britvin *et al.* 1999). The composition of rhodarsenide included in olivine (anal. 1200B–2–6, Table 4, Fig. 5C) shows considerable substitution of Pd for Rh and leads to the formula $(Rh_{1.55}Pd_{0.34}Ru_{0.02}Ni_{0.02}Fe_{0.04})_{\Sigma 1.95}As_{1.01}$. Two compositions from inclusions in chromite (anal. BV27C–4–3 and TW23A–2–1, Table 4, Figs. 5E, D) have Pd higher than Rh and give the formulae $Rh(Pd_{1.09}Rh_{0.92}Ru_{0.02})_{\Sigma 2.03}As_{0.96}$ and $(Pd_{1.16}Rh_{0.72}Ru_{0.07}Ni_{0.03})_{\Sigma 1.98}As_{1.01}$, respectively. They may be members of the rhodarsenide–palladodymite solid solution (Britvin *et al.* 1999), although this attribution cannot be conclusive without structural data. The composition $(Pd_{0.99}Rh_{0.98}Ni_{0.02}Cu_{0.01})_{\Sigma 2}(As_{0.72}Sb_{0.27})_{\Sigma 0.99}$ from the olivine-hosted polyphase inclusion (anal. 1200B–1–8, Table 4, Fig. 5B) is characterized by substantial substitution of Sb for As and possibly represents a Sb-rich variety of palladoarsenide or palladodymite. The monoarsenide-type compounds were classified as possible members of the solid solution between cherepanovite (orthorhombic RhAs, Rudashevsky *et al.* 1985) and ruthenarsenite (orthorhombic RuAs, Harris 1974). The Ru-rich cherepanovite (Fig. 5B) and Rh-rich ruthenarsenite (Fig. 5D) correspond to the formulae $(Rh_{0.53}Ru_{0.46})_{\Sigma 0.99}As_1$ and $(Ru_{0.57}Rh_{0.41}Pd_{0.02})_{\Sigma 1}(As_{0.96}S_{0.03})_{\Sigma 0.99}$, respectively (anal. 1200B–1–10 and TW23A–2–2, Table 4). Single-phase ruthenarsenite (Fig. 5A) is Pd-free and exhibits a relatively high Ru:Rh ratio $(Ru_{0.69}Rh_{0.29})_{\Sigma 0.98}As_{0.99}$ (anal. 1200A–1–2, Table 4).

Sperrylite

Sperrylite in the type-3 assemblage (Fig. 6A) has an average composition corresponding to the stoichiometry $(Pt_{0.96}Ru_{0.02})_{\Sigma 0.98}As_{1.98}$, although it shows a remarkable decrease in Rh from core to rim (anal. 1200C–1–1 and 1200C–1–3, Table 4).

Hollingworthite

Hollingworthite in the type-3 assemblage (Fig. 6B) is slightly heterogeneous in composition (anal. 1201A–1–2 and 1201A–1–4), varying from $(Rh_{0.77}Pt_{0.13}Os_{0.04}Ru_{0.03})_{\Sigma 0.97}(As_{1.12}S_{0.91})_{\Sigma 2.03}$ to $(Rh_{0.68}Pt_{0.16}Os_{0.07}Ru_{0.07}Pd_{0.01})_{\Sigma 0.99}(As_{1.08}S_{0.93})_{\Sigma 2.01}$.

Irarsite

The single-phase grain of irarsite from sample BV27C–3a could be identified only qualitatively because of its small size, less than 2 μm.

Unidentified Pd antimonide

The Pd–Sb compound from the type-2 composite inclusion of Figure 5D could not be quantitatively defined, although X-ray spectral data suggest stibiopalladinite (ideal Pd_5Sb_2) or sudburyite, ideally (Pd,Ni)Sb.

DISCUSSION

There has been considerable debate regarding the origin of the ultramafic pipes in the Bushveld Complex. With regard to the iron-rich bodies, a magmatic origin has been favored by Viljoen & Scoon (1985), the magma having been derived from within the pile of cumulates either as a residual liquid or as an immiscible

silicate liquid. On the basis of the distinctive and uniform initial Sr-isotope ratio and high temperature of formation of the clinopyroxene of the pipes, regardless of stratigraphic height, Cawthorn *et al.* (2000) questioned an origin from within the layered sequence, and suggested that the pipes resulted from the injection of new magma. In contrast, the high chlorine content of hydrous minerals in one of the pipes (Driekop) led Schiffries (1982) to appeal to a hydrothermal fluid causing the desilication of orthopyroxenite to yield dunite and the introduction of PGE as chloride complexes. Several lines of evidence indicate that the Tweefontein pipe was forcefully intruded as a relatively dense silicate melt able to transport and displace upward fragments of the MG chromitites by about 125 m, although the presence of replacive clinopyroxenite might indicate relatively high activity of volatile-rich fluids that would have favored assimilation and metasomatic reaction with the country rocks (Tegner *et al.* 1994). In the Onverwacht pipe, there is evidence for a collapse of the LG6 chromitite and associated layers around the pipe body, by about 80 m (Fig. 2) suggesting local derivation of the material within the pipe. In spite of the fact that petrogenetic aspects of the pipes at Onverwacht and Tweefontein remain open to question, there is convincing evidence that the chromitite bodies in these pipes are fragments of the LG6 and MG4 chromitite layers, respectively (Wagner 1929, Tegner *et al.* 1994). Chromitite fragments from both localities have identical PGM assemblages, which, however, differ remarkably from the PGM assemblages in undisturbed chromitite layers LG6 and MG4.

Generally speaking, LG and MG chromitites are characterized by a low PGE content, and they display a quite monotonous PGM assemblage dominated by laurite and minor cooperite (Maier *et al.* 1999, and Table 5). This relatively high abundance of laurite would be consistent with type-1 assemblage of the PGM in chromitite xenoliths, although comparison of laurite composition in terms of Ru–Os–Ir atomic proportions (Fig. 7) indicates that there is only partial overlap of compositions close to the Ru apex of the diagram. The xenolith-hosted laurite has an even more Ru-rich and Ir-poor composition relative to that from LG and MG chromitites. Furthermore, significant, although scattered, As enrichment distinguishes the laurite in the xenoliths (Table 3) from laurite in undisturbed LG6 and MG layers, which usually has As below the detection limit (Table 5).

The PGM assemblages of type 2 and 3 in the xenoliths are not found in undisturbed LG and MG chromitite layers. They bear some similarity with the PGM associations reported from either mineralized iron-rich dunites at Mooihoek and Onverwacht (Rudashevsky *et al.* 1992), or mining concentrates, presumably derived from the same type of mineralized dunites, at Driekop (Tarkian & Stumpfl 1975). Both chromitite xenoliths and platiniferous dunites display a clear predominance of Pt–Fe alloys, arsenides and sulfarsenides over sulfides.

The isoferroplatinum from Onverwacht and Tweefontein is slightly Pt-deficient and possibly formed by unmixing from an original homogeneous Pt–Ru–Fe alloy. According to Rudashevsky *et al.* (1992), isoferroplatinum is syngenetic with olivine in platiniferous dunites, whereas arsenides and sulfarsenides crystallized with clinopyroxene and Ti-rich magnetite. We noted the same order of crystallization in the xenoliths; alloys and compounds of As occur together in composite grains included in fresh chromite and olivine at a high-temperature stage. Rudashevsky *et al.* (1992) described sperrylite and hollingworthite as being syngenetic with late amphiboles, chlorite and oxides in platiniferous dunites, however. This is possibly also the case for type-

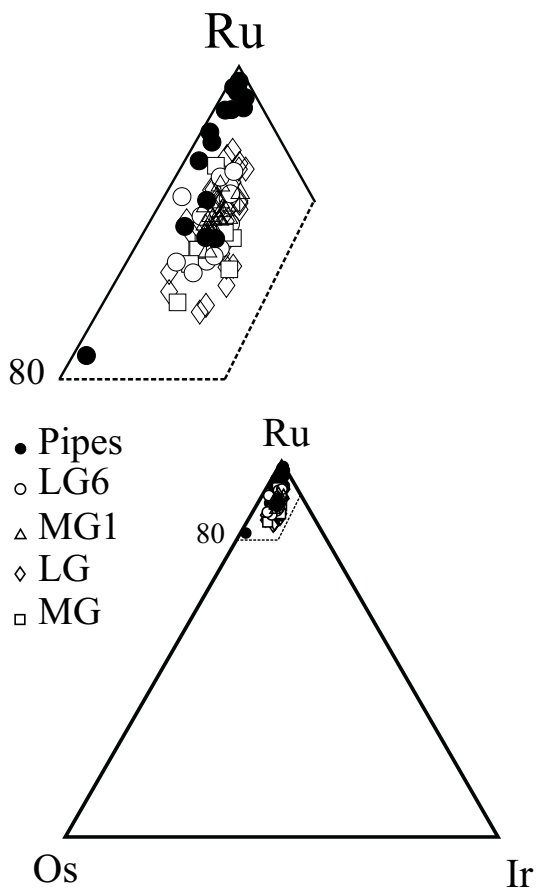

FIG. 7. Projection of laurite compositions (at.%) in Ru–Os–Ir ternary diagram. Diamond: LG chromitites, square: MG chromitites (data from Maier *et al.* 1999), circle: LG6 chromitite, triangle: MG1 chromitite (present work), dot: chromitite xenoliths from the Tweefontein and Onverwacht pipes (present work).

TABLE 5. REPRESENTATIVE COMPOSITIONS OF LAURITE IN CHROMITITE LAYERS FROM THE BUSHVELD COMPLEX

		Os	Ir	Ru	Rh	Pt	Pd	Ni	Fe	Cu	S	As	Total
LG6 chromitite layer													
BV20ge 1 1	wt%	7.14	2.85	46.98	0.62	0.00	0.74	0.22	0.19	0.09	38.31	0.00	97.12
BV20ge 3 1		7.19	4.22	52.66	0.28	0.00	0.33	0.05	0.04	0.02	35.63	0.00	100.41
BV20ge 4 1		5.89	4.61	51.63	1.42	0.00	0.08	0.14	0.24	0.05	35.98	0.00	100.03
BV20ge 6 2		5.65	3.50	54.51	0.41	0.00	0.39	0.04	0.07	0.00	35.70	0.00	100.26
BV21ge 4 1		7.98	4.84	46.30	0.68	0.00	0.63	0.06	0.03	0.00	36.73	0.00	97.24
BV21ge 7 1		6.61	4.21	51.01	0.30	0.00	0.74	0.08	0.03	0.00	35.77	0.00	98.75
BV24ge 10 1		9.03	4.97	48.41	1.57	b.d.l.	0.14	0.02	0.00	0.04	36.76	0.00	100.93
BV24ge 5 1		6.27	4.92	49.72	1.47	0.00	0.06	0.18	0.46	0.00	37.34	0.00	100.41
BV24ge 9 1		5.68	4.24	53.79	0.69	0.00	0.42	0.13	0.36	0.00	35.44	0.00	100.75
MG1 chromitite layer													
BV26A 1 1		7.25	4.24	51.45	0.00	b.d.l.	0.26	0.08	0.00	0.01	34.86	0.00	98.13
BV26A 3 3		7.45	3.90	53.01	0.40	0.00	0.14	0.11	0.00	0.00	35.08	0.00	100.09
BV26A 4 1		6.75	5.15	48.01	1.96	0.00	0.00	0.01	0.00	0.03	35.63	0.00	97.55
BV26A 5 2		6.34	5.55	49.55	1.05	0.00	0.29	0.07	0.00	0.01	37.14	0.00	100.01
BV26B 1 2		7.66	6.46	46.92	2.13	0.00	0.49	0.06	0.00	0.00	36.16	0.00	99.88
BV26B 5 1		7.03	4.65	48.37	2.22	0.00	0.00	0.12	0.70	0.00	35.11	0.00	98.19
BV26c 1 1		4.85	4.41	52.98	1.10	b.d.l.	0.00	0.09	0.00	0.11	35.53	0.00	99.07
BV26c 2 1		6.93	4.03	53.16	0.00	0.00	0.00	0.03	0.00	0.00	36.44	0.00	100.59
BV26c 2 2		7.16	4.02	53.18	0.00	0.00	0.00	0.08	0.04	0.00	36.92	0.00	101.40
BV26c 6 1		7.02	3.23	53.02	0.69	b.d.l.	0.00	0.06	0.18	0.00	36.46	0.00	100.66
BV26c 6 2		6.90	4.21	51.04	0.66	b.d.l.	0.00	0.11	0.18	0.02	36.66	0.00	99.78
BV26c 7 1		6.59	4.87	52.61	0.52	b.d.l.	0.00	0.17	0.45	0.01	35.70	0.00	100.92
BV26c 8 2		7.18	4.57	51.18	0.47	0.00	0.00	0.16	0.91	0.00	36.36	0.00	100.83
BV26c 8 3		7.04	4.86	52.24	0.00	b.d.l.	0.08	0.19	0.42	0.00	35.99	0.00	100.82
BV26c 9 1		7.73	4.13	52.35	0.00	0.00	0.00	0.17	0.18	0.00	35.48	0.00	100.04
BV26c 9 2		7.93	3.79	49.70	b.d.l.	0.27	0.82	0.14	0.18	0.00	35.93	0.00	98.76
BV26c 9 3		6.94	3.88	51.34	0.50	0.00	0.00	0.13	0.14	0.01	35.93	0.00	98.87
BV26ge 4 1		7.88	3.89	48.30	0.29	0.00	0.97	0.11	0.05	0.00	38.16	0.00	99.64
BV26ge 6 1		6.18	3.76	53.93	b.d.l.	0.00	0.62	0.17	0.33	0.02	37.22	0.00	102.22
BV26ge 8 1		6.06	3.42	48.85	0.85	0.00	0.64	0.17	0.13	0.00	37.48	0.00	97.59
BV26ge 8 2		6.41	3.51	52.42	0.35	0.26	0.65	0.19	0.28	0.00	36.96	0.00	101.02

3 assemblages in the xenoliths, in which sperrylite and hollingworthite are closely associated with secondary phases produced by alteration, although we cannot exclude that they crystallized at high temperature and have come in contact with secondary minerals during low-temperature alteration of the chromite host.

Mineralogical differences between the PGM in the chromitite layers and those reported from the xenoliths may be interpreted as a result of metasomatic reaction with fluid or melt occupying the pipe. In this view, the laurite-rich inclusions from the xenoliths may represent partially reworked relics of the original PGM assemblage, whereas the complex association of PGM enriched in As, Pd, Rh, and Pt appears to be consanguineous with the PGE mineralization in the dunites. It is possible, therefore, that the (As,Pd,Rh,Pt)-bearing PGM were contributed to the chromitite xenoliths by the pipe component, whether it was a metasomatic fluid or a true silicate magma. Since the PGM inclusions in the xenoliths occur encapsulated in fresh chromite and olivine, we conclude that they did not precipitate from solutions circulating along cracks and fissures, but crystallized early at a high temperature prior to or together with their mineral hosts. This model necessarily implies that the xenoliths have undergone an important metasomatism capable of completely recrystallizing chromite and olivine, and with substantial reworking of the original PGM inclusions. The compositional re-equilibration of the chromite in the xenoliths supports this conclusion (Stumpfl & Rucklidge 1982, Tegner *et al.* 1994).

The effects of metasomatism from the replacement-type ultramafic pipes have already been reported for UG1 and UG2 chromitite layers occurring adjacent to (and beyond) the ultramafic pipes (McLaren & De Villiers 1982, Peyerl 1982, Merkle 1988). These altered chromitites are characterized by an abundance of Pt–Fe

LG6 chromitite layer

BV20ge 1 1	at.%	2.16	0.86	26.81	0.34	0.00	0.40	0.22	0.20	0.08	68.92	0.00
BV20ge 3 1		2.22	1.29	30.65	0.16	0.00	0.18	0.05	0.04	0.01	65.38	0.00
BV20ge 4 1		1.81	1.40	29.87	0.81	0.00	0.04	0.14	0.25	0.04	65.63	0.00
BV20ge 6 2		1.74	1.06	31.54	0.23	0.00	0.22	0.04	0.07	0.00	65.10	0.00
BV21ge 4 1		2.49	1.49	27.19	0.39	0.00	0.35	0.06	0.03	0.00	68.00	0.00
BV21ge 7 1		2.06	1.30	29.89	0.17	0.00	0.41	0.08	0.03	0.00	66.06	0.00
BV24ge 10 1		2.77	1.51	27.92	0.89	0.00	0.07	0.02	0.00	0.03	66.79	0.00
BV24ge 5 1		1.89	1.47	28.25	0.82	0.00	0.03	0.18	0.47	0.00	66.88	0.00
BV24ge 9 1		1.75	1.29	31.15	0.39	0.00	0.23	0.12	0.38	0.00	64.68	0.00

MG1 chromitite layer

BV26A 1 1	2.29	1.33	30.65	0.00	0.00	0.15	0.09	0.00	0.01	65.49	0.00
BV26A 3 3	2.32	1.20	31.13	0.23	0.00	0.08	0.11	0.00	0.00	64.93	0.00
BV26A 4 1	2.13	1.61	28.47	1.14	0.00	0.00	0.01	0.00	0.03	66.61	0.00
BV26A 5 2	1.93	1.67	28.42	0.59	0.00	0.16	0.07	0.00	0.01	67.15	0.00
BV26B 1 2	2.38	1.98	27.43	1.22	0.00	0.28	0.06	0.00	0.00	66.65	0.00
BV26B 5 1	2.21	1.45	28.65	1.29	0.00	0.00	0.12	0.75	0.00	65.53	0.00
BV26c 1 1	1.50	1.35	30.93	0.63	0.00	0.00	0.09	0.00	0.10	65.39	0.00
BV26c 2 1	2.12	1.22	30.57	0.00	0.00	0.00	0.03	0.00	0.00	66.06	0.00
BV26c 2 2	2.17	1.20	30.26	0.03	0.00	0.00	0.08	0.04	0.00	66.22	0.00
BV26c 6 1	2.14	0.97	30.37	0.39	0.00	0.00	0.06	0.19	0.00	65.88	0.00
BV26c 6 2	2.11	1.27	29.44	0.37	0.00	0.00	0.11	0.19	0.02	66.49	0.00
BV26c 7 1	2.03	1.48	30.42	0.30	0.00	0.00	0.17	0.47	0.01	65.12	0.00
BV26c 8 2	2.19	1.38	29.35	0.26	0.00	0.00	0.16	0.94	0.00	65.72	0.00
BV26c 8 3	2.16	1.48	30.16	0.00	0.00	0.04	0.19	0.44	0.00	65.53	0.00
BV26c 9 1	2.40	1.27	30.60	0.00	0.00	0.00	0.17	0.19	0.00	65.37	0.00
BV26c 9 2	2.47	1.17	29.11	0.00	0.06	0.46	0.14	0.19	0.00	66.40	0.00
BV26c 9 3	2.15	1.19	29.97	0.29	0.00	0.00	0.13	0.15	0.01	66.11	0.00
BV26ge 4 1	2.38	1.16	27.40	0.16	0.00	0.52	0.11	0.05	0.00	68.23	0.00
BV26ge 6 1	1.84	1.11	30.26	0.00	0.00	0.33	0.16	0.34	0.02	65.94	0.00
BV26ge 8 1	1.85	1.03	28.08	0.48	0.00	0.35	0.16	0.13	0.00	67.91	0.00
BV26ge 8 2	1.93	1.05	29.76	0.19	0.07	0.35	0.18	0.29	0.00	66.16	0.00

Results of electron-microprobe analyses, quoted in weight % above and in terms of atom proportions below. b.d.l.: below detection limit. Detection limits as stated in Table 3.

alloys and Pt–Rh–Pd arsenides similar to the xenoliths. In particular, Merkle (1988) reported an increase in the proportion of Pt–Fe alloy within the UG1 chromitites affected by metasomatizing fluids. McLaren & De Villiers (1982) described an increase in modal abundance of Pt–Fe alloys in the PGM assemblage of UG2 adjacent to a discordant ultramafic "pegmatoid" at Maandagshoek. Peyerl (1982) observed similar changes in PGM of UG2 chromitites with distance from the Driekop pipe, and Penberthy & Merkle (1999) recognized in the same chromite layer the effects of interaction with "pegmatoid" capable of affecting the pristine PGM. Furthermore, in the UG2 chromitite in proximity to a pipe at the Western Platinum mine near Marikana (western Bushveld), Grimbeek (1995) documented a clear variation from PGE in sulfide minerals in pristine chromitite to a greater proportion of alloys, arsenides, tellurides and sulfarsenides with increasing interaction with components at the pipe. These variations in the PGM assemblage are consistent with the results obtained here for the Onverwacht and Tweefontein chromitite xenoliths, although we have not found tellurides.

The scarcity of PGM sulfides and the common occurrence of As-bearing species and PGE alloys is an ubiquitous feature in the platiniferous dunites, the chromitite xenoliths, and in the metasomatized fragments of chromitite. They indicate that crystallization in the pipe was characterized by conditions of low sulfur fugacity, and relatively high As:S ratio, as was also invoked by Rudashevsky *et al.* (1992) for the precipitation of PGM in platiniferous dunites at Mooihoek and Onverwacht. The important role played by an As-rich melt to concentrate the PGE has been previously reported by Merkle (1992). In his model, the evidence for such an As-rich melt as a collector can be preserved only in conditions of low fugacity of sulfur, or if the time between the formation of As-rich melt and later saturation in sulfide is quite long.

Conclusions

In this paper, we have presented the results of a mineralogical investigation of PGM inclusions in chromitite fragments from the ultramafic pipes of Tweefontein and Onverwacht, in the eastern part of the Bushveld complex. The major conclusions are:

1) The small number of PGM grains encountered does not account for the very high grade of PGE (approximately 1700 ppm) reported by Wagner (1929) for a sample of chromitite from the Onverwacht dunitic pipe. This may be possibly due to limitations of our sampling or the nugget effect in PGE analysis by Wagner (1929).

2) The chromitite xenoliths display PGM assemblages substantially modified by metasomatic reaction in the pipe component with respect to those in undisturbed layers of chromitite, considered to be the source of the xenoliths. Important changes involve a decrease in PGM sulfides and an increase in PGE alloys and PGM arsenides and sulfarsenides, indicative of low fugacity of sulfur and high As/S in metasomatizing fluids related to the pipe.

3) Given the lack of total PGE analyses, we could not establish whether the metasomatic process produced an increase of the PGE content or a simple reworking of existing PGM in the chromitite xenoliths. Comparison with PGM assemblages in the chromitite layers suggest that Pt, Pd, and Rh were added together with As and Sb during the metasomatic event.

4) The textural position of the metasomatic PGM, included in fresh chromite and olivine, implies that the interaction of the chromitite layers with the up-welling pipe magma may have occurred when the chromitites were still hot and not completely solidified.

Acknowledgements

Mine management and geologists at Eastern Chrome and Samancor are thanked for information regarding the structure of the chromitite adjacent to the Onverwacht pipe, and for their and Anglo Platinum's permission to publish these results. RGC's research is supported by Anglo Platinum, Lonmin, Impala Platinum and the National Research Foundation. R.W. Merkle, C. Tegner, N.J. Cook, and R.F. Martin are thanked for their useful suggestions and thorough revision of the manuscript. The authors are grateful to E. Galli for providing XRD data on mcguinnessite, and to M. Tonelli and G. D'Urso of the CIGS (Modena University) for their assistance during SEM work. This paper is contributed in honor of Louis Cabri on the occasion of his retirement.

References

Begizov, V.D., Meshchankina, V.I. & Dubakina, L.S. (1974): Palladoarsenide, Pd_2As, a new natural palladium arsenide from the copper–nickel ores of the Oktyabr'skiy deposit. *Vses. Mineral. Obshchest.* **103**, 104-107 (in Russ.).

Brenan, J.M. & Andrews, D. (2001): High-temperature stability of laurite and Ru–Os–Ir alloy and their role in PGE fractionation in mafic magmas. *Can. Mineral.* **39**, 341-360.

Britvin, S.N., Rudashevsky, N.S., Bogdanova, A.N. & Shcherbachev, D.K. (1999): Palladodymite $(Pd,Rh)_2As$, a new mineral from a placer of the Miass river, the Urals. *Zap. Vser. Mineral. Obshchest.* **128**(2), 39-42 (in Russ.).

Cabri, L.J. & Chen, T.T. (1976): Stibiopalladinite from the type locality. *Am. Mineral.* **61**, 1249-1254.

_____ & Feather, C.E. (1975): Platinum–iron alloys: a nomenclature based on a study of natural and synthetic alloys. *Can. Mineral.* **13**, 117-126.

_____, Laflamme, J.H.G. & Stewart, J.M. (1977b): Platinum-group minerals from Onverwacht. II. Platarsite. A new sulfarsenide of platinum. *Can. Mineral.* **15**, 385-388.

_____, _____, _____, Rowland, J.F. & Chen, T.T. (1975): New data on some palladium arsenides and antimonides. *Can. Mineral.* **13**, 321-335.

_____, Rosenzweig, A. & Pinch, W.W. (1977a): Platinum-group minerals from Onverwacht. I. Pt–Fe–Cu–Ni alloys. *Can. Mineral.* **15**, 380-384.

_____, Stewart, J.M., Laflamme, J.H.G. & Szymański, J.T. (1977c): Platinum-group minerals from Onverwacht. III. Genkinite $(Pt,Pd)_4Sb_3$, a new mineral. *Can. Mineral.* **15**, 389-392.

Cawthorn, R.G. (1999): The discovery of the platiniferous Merensky Reef in 1924. *S. Afr. J. Geol.* **102**(3), 178-183.

_____, Harris, C. & Kruger, F.J. (2000): Discordant ultramafic pegmatoidal pipes in the Bushveld Complex. *Contrib. Mineral. Petrol.* **140**, 119-133.

Donovan, J.J. & Rivers, M.L. (1990): PRSUPR – a PC based automation and analyses software package for wavelength dispersive electron beam microanalysis. *Microbeam Anal.*, 66-68.

Grimbeek, J.C. (1995): *The Effect of the Vaalkop Replacement Pegmatoid on the Sulphide Mineralogy at Western Platinum Mine in the Mooinooi District*. M.Sc. thesis, Univ.of Pretoria, Pretoria, South Africa.

HARRIS, D.C. (1974): Ruthenarsenite and iridarsenite, two new minerals from the Territory of Papua and New Guinea and associated irarsite, laurite and cubic iron-bearing platinum. *Can. Mineral.* **12**, 280-284.

_____ & CABRI, L.J. (1991): Nomenclature of platinum-group-element alloys: review and revision. *Can. Mineral.* **29**, 231-237.

MAIER, W.D, PRICHARD, H.M, FISHER, P.C. & BARNES S.-J. (1999): Compositional variation of laurite at Union Section in the Western Bushveld Complex. *S. Afr. J. Geol.* **102**(3), 286-292.

MCLAREN, C.H. & DE VILLIERS, J.P.R. (1982): The platinum-group chemistry and mineralogy of the UG–2 chromitite layer of the Bushveld Complex. *Econ. Geol.* **77**, 1348-1366.

MEADON, S.B. (1995): *Physical and Chemical Properties of the MG1 Chromitite Layers, Tweefontein Mine, Bushveld Complex*. M.Sc. thesis, Univ. of the Witwatersrand, Johannesburg, South Africa.

MERKLE, R.K.W. (1988): The effects of metasomatising fluids on the PGE-content of the UG–1 chromitite layer. *In* Geo-Platinum 87 (H.M. Prichard, P.J. Potts, J.F.W. Bowles & S.J. Cribb, eds.). Elsevier, London, U.K. (359-360).

_____ (1992): Platinum-group minerals in the middle group of chromitite layers at Marikana, western Bushveld Complex: indications for collection mechanism and postmagmatic modification. *Can. J. Earth Sci.* **29**, 209-221.

PENBERTHY, C.J. & MERKLE, R.K.W. (1999): Lateral variations in the platinum-group element content and mineralogy of the UG–2 chromitite layer, Bushveld Complex. *S. Afr. J. Geol.* **102**(3), 240-250.

PEYERL, W. (1982): The influence of the Driekop dunite pipe on the platinum-group mineralogy of the UG–2 chromitite in its vicinity. *Econ. Geol.* **77**, 1432-1438.

RUDASHEVSKY, N.S., AVDONTSEV, S.N. & DNEPROVSKAYA, M.B. (1992): Evolution of PGE mineralization in hortonolitic dunites of the Mooihoek and Onverwacht pipes, Bushveld Complex. *Mineral. Petrol.* **47**, 37-54.

_____, MOCHALOV, A.G., TRUBKIN, N.V., SHUMSKAYA, N.I., SHKURSKIY, V.I. & EVSTIGNEEVA, T.L. (1985): Cherepanovite, RhAs, a new mineral. *Zap. Vses. Mineral. Obshchest.* **114**, 464-469 (in Russ.).

SCHIFFRIES, C.M. (1982): The petrogenesis of a platiniferous dunite pipe in the Bushveld Complex: infiltration metasomatism by a chloride solution. *Econ. Geol.* **77**, 1439-1453.

SCOON, R.N. & TEIGLER, B. (1994): Platinum-group element mineralization in the Critical Zone of the western Bushveld Complex. I. Sulfide poor-chromitites below the UG–2. *Econ. Geol.* **89**, 1094-1121.

_____ & _____ (1995): A new LG–6 chromite reserve at Eerste Geluk in the boundary zone between the central and southern sectors of the eastern Bushveld Complex. *Econ. Geol.* **90**, 969-982.

STUMPFL, E.F. & RUCKLIDGE, J.C. (1982): The platiniferous dunite pipes of the eastern Bushveld. *Econ. Geol.* **77**, 1419-1431.

TARKIAN, M., KRSTIĆ, S., KLASKA, K.H. & LIESSMANN, W. (1997): Rhodarsenide, $(Rh,Pd)_2As$, a new mineral. *Eur. J. Mineral.* **9**, 1321-1325.

_____ STUMPFL, E.F. (1975): Platinum mineralogy of the Driekop mine, South Africa. *Mineral. Deposita* **10**, 71-85.

TEGNER, C., WILSON, J.R. & CAWTHORN, R.G. (1994): The dunite–clinopyroxenite pegmatoidal pipe, Tweefontein, eastern Bushveld complex, South Africa. *S. Afr. J. Geol.* **97**, 415-430.

VILJOEN, M.J. & HIEBER, R. (1986): The Rustenburg section of Rustenburg Platinum Mines Ltd., with reference to the Merensky Reef. *In* Mineral Deposits of Southern Africa **II** (C.R. Anhaeusser & S. Maske, eds.). The Geological Society of South Africa, Johannesburg, South Africa (1107-1134).

_____ & SCOON, R.N. (1985): The distribution and main geologic features of discordant bodies of iron-rich ultramafic pegmatite in the Bushveld Complex. *Econ. Geol.* **80**, 1109-1128.

WAGNER, P.A. (1929): *The Platinum Deposits and Mines of South Africa*. Oliver & Boyd, Edinburgh, U.K.

_____ & MELLOR, E.T. (1925): On platinum-bearing hortonolite-dunite of the Lydenburg District. *Trans. Geol. Soc. S. Afr.* **28**, 1-18.

Received November 28, 2000, revised manuscript accepted August 11, 2001.